Thermochemical process for seasonal storage of solar energy: characterization and modeling of a high-density reactive bed

Benoit Michel, Nathalie Mazet, Sylvain Mauran, Driss Stitou, Jing Xu

Thermochemical process for seasonal storage of solar energy: characterization and modeling of a high-density reactive bed

Benoit Michel[a,*], Nathalie Mazet[a], Sylvain Mauran[a,b], Driss Stitou[a], Jing Xu[a]

[a] PROMES-CNRS, Tecnosud, Rambla de la thermodynamique, 66100 Perpignan, France
[b] Université de Perpignan Via Domitia, 52 Av. Paul Alduy, 66860 Perpignan, France

Abstract:
This paper focuses on the characterization and modeling of a solid/gas thermochemical reaction between a porous reactive bed and moist air flowing through it. The aim is the optimization of both energy density and permeability of the reactive bed, in order to realize a high density thermochemical system for seasonal thermal storage for house heating application. Several samples with different implementation parameters (density, binder, diffuser, porous bed texture) have been tested. Promising results have been reached: energy densities about 430-460 kWh.m^{-3} and specific powers between 1.93 and 2.88 W.kg^{-1} of salt. A model based on the assumption of a sharp reaction front moving through the bed during the reaction was developed. It has been validated by a comparison with experimental results for several reactive bed samples and operating conditions.

Keywords:
Thermochemical process, seasonal thermal storage, sharp front model, high-density reactive salt, permeability.

* Corresponding author:
E-mail: michel.benoit@promes.cnrs.fr

Nomenclature:

Dec	energy density, $J.m^{-3}$	μ	air viscosity, $Pa.s$
h	molar enthalpy, $J.mol^{-1}$	v	stoichiometric coefficient, mol_G/mol_s
j	molar flow, $mol.m^{-2}.s^{-1}$	ρ	density, $kg.m^{-3}$
k	permeability, m^2	Ω	cross section of the salt bed, m^2
K	equilibrium constant		
M	molar weight, $kg.mol^{-1}$	*Indices*	
m	mass, kg	0	dehydrated salt
n	molar density, $mol.m^{-3}$	1	hydrated salt
N	mole quantity of salt, mol	a	dry air
$\dot{n}$	sink or source of gas, $mol.s^{-1}$	$eqLG$	liquid/gas equilibrium
p	pressure, Pa	$eqSG$	solid / gas equilibrium
P_m	specific power, $W.kg^{-1}$	f	at the reaction front
Δp	pressure drop across the salt bed, Pa	G	gas
R	gas constant, $J.mol^{-1}.K^{-1}$	h	moist air
T_c	constraint temperature, K	i	inlet of the porous bed
$\boldsymbol{u}$	velocity vector, $m.s^{-1}$	j	outlet of the porous bed
$\dot{V}$	flow rate, $m^3.h^{-1}$	s	salt
X	reaction advancement	sh	sample holder
Z	Thickness, m	t	total
		v	water vapor
Greek symbols		X	reaction advancement
Δh_r^0	standard enthalpy of reaction, $J.mol^{-1}_G$		
Δs_r^0	standard entropy of reaction, $J.mol^{-1}_G.K^{-1}$	*Exponents*	
ε	porosity	0	reference

Introduction

In France, the energy needs for residential use represent 43% of the national energy consumption and 25% of greenhouse gas emissions [1]. The European community has decided a challenging energy policy focused on a target: the "3 times 20 target" (20 per cent less greenhouse gases compared to 1990, 20 per cent better energy efficiency, and a 20 per cent share of renewable). The use of renewable energies and in particular solar energy for household applications is a key issue to reach this target and more generally for decrease the high energy consumption and the greenhouse gas emissions in the residential sector worldwide.

In order to maximize the use of solar energy for house heating, it is interesting to valorize the solar energy excess in summer using a long-term storage (3-6 months). Such a seasonal storage system for house heating must have on one hand the lowest heat losses between summer and winter, and on the other hand, the smaller volume i.e. the highest energy density.

The thermal energy storage can be classified in three storage mechanisms: based on sensible heat, latent heat, and thermochemical processes. There are several studies about seasonal storage for residential applications with these different mechanisms [2, 3]. Nevertheless, the thermochemical storage takes advantage of a high storage density (about 200 to 500 $kWh.m^{-3}$), and negligible heat losses between the storage period and the recovery period because the energy is stored as chemical potential, and the sensible heat of the elements is weak. Therefore, this kind of storage is relevant for seasonal storage for house heating. As a matter of comparison, the energy density of latent storage is about 90 $kWh.m^{-3}$ and the energy density of sensible water is about 54 $kWh.m^{-3}$ (for a ΔT of 70 °C and heat losses of 25%) [4].

Such thermochemical storage process involves a reversible chemical reaction between a solid and a gas (the solid/gas pair under study in this paper is a hydrate/water pair). The synthesis (or hydration) of the solid is exothermic (heating stage), while its decomposition (or dehydration) requires a heat input (storage stage). Most of thermochemical systems operate with pure steam [5-10], but the feasibility and value of systems running with moist air is currently investigated [11-15], and seems to be promising [16]. However, up to date there is no completed seasonal storage based on a thermochemical process [3].

Beside the high storage density criteria, a seasonal storage system has also to fulfill requirements about thermal power production for the heat recovery step. To define a target value for this thermal power, an acceptable range for the mass of salt is fixed (5 to 10 tons) and a typical French climate and an efficient house are chosen (as SFH100, see [17]). The mean thermal power required for heating is about: 3.5 kW [17, 18], and, consequently, the thermal specific power of the salt ranges between: 0.3 to 0.7 $W.kg^{-1}$.

For such large thermal storages, the simplest and cheapest reactor configuration has to be defined. Thus, according to PROMES laboratory knowledge [19, 20], a fixed bed configuration is chosen and different ways to implement the reactive salt are investigated.

Let's recall that the storage density depends on the density of the reactive bed, and the thermal power depends on the kinetics and heat and mass transfers through the bed. Moreover, Lu et al. showed [21] that for reactive bed at high density, the mass transfers through the bed are a key point. Thus, the various implementations under study aim at increasing the energy density of the reactive bed (by compacting it), but without penalizing mass transfers (by selecting texture parameters such as grain size, by adding a porous binder or a gas diffuser).

The objective of this work is first to characterize the mass transfer within the reactive salt bed, especially in measuring the reaction kinetics and the permeability of the porous bed according to these implementation parameters (density, ratio of binder, porosity, diffusers). Secondly, a model is developed to represent the transformation of the reactive bed and, consequently, to estimate the recovered thermal power.

The aim is to optimize both the density and permeability of the salt bed, in order to obtain a porous reactive bed that maximizes the storage energy density and fulfils the target value of thermal power. It is worth noting that these two characteristics, density and permeability, evolve in an antagonistic way.

2. Principle of solid/gas sorption processes for seasonal heat storage

2.1. Solid / gas process

The thermochemical process is based on the thermal effect of a monovariant reversible reaction between a solid and a reactive gas.

$$S_0 + \nu G \leftrightarrows S_1 + \nu(\Delta h_r^0) \tag{1}$$
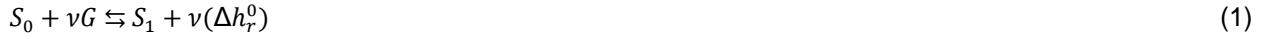
The equilibrium conditions (p_{eqSG}, T_{eqSG}) of the solid/gas reaction follow the Clausius-Clapeyron relation. This relation is obtained by stating that the free Gibbs energy, for this transformation, is equal to zero at the thermodynamic equilibrium:

$$\Delta G_r = \Delta G_r^0 + RT_{eqSG}lnK = \nu\Delta h_r^0 - \nu T_{eqSG}\Delta s_r^0 + RT_{eqSG}lnK = 0 \tag{2}$$

K is the equilibrium constant for the solid/gas reaction. Assuming the reactive gas behaves as perfect gas, K becomes:

$$K = \left(\frac{p_{eqSG}}{p^0}\right)^\nu \tag{3}$$

Δh_r^0 and Δs_r^0 are respectively the standard enthalpy and entropy of the solid/gas reaction and p^0 is the reference pressure (1 bar).

Finally, the thermodynamic equilibrium conditions are determined by only one intensive variable: the equilibrium gas pressure p_{eqSG} or the equilibrium temperature of the bed T_{eqSG}:

$$ln\left(\frac{p_{eqSG}}{p^0}\right) = -\frac{\Delta h_r^0}{R\,T_{eqSG}} + \frac{\Delta s_r^0}{R} \tag{4}$$

2.2. Solid / gas pair for seasonal thermochemical storage

To avoid environmental risks, a hydrate/water pair is selected as reactant. The working conditions are defined by the use of this storage process for house heating:

- for the storage step: the decomposition phase of the hydrate (S_1) is carried out using a solar collector as heat input source at T < 90 °C
- for the recovery step : the synthesis reaction of S_1 supplies heat at a temperature beyond 35 °C, for heating purpose; the water vapor pressure is at least at 1200 Pa (corresponding to an evaporation temperature of winter at 10 °C).

Strontium bromide fulfills these conditions and has been chosen. It was already identified and used for similar applications [5, 8, 22]. The reaction is:

$$<SrBr_2, 1H_2O> + 5(H_2O) \leftrightarrow <SrBr_2, 6H_2O> + 5\Delta h^0_r \tag{5}$$

The $<SrBr_2, 1H_2O>$ and the $<SrBr_2, 6H_2O>$ are respectively the dehydrated (S_0) and hydrated (S_1) salts and the water is the reactive gas (G).

The reaction advancement is defined by the following ratio:

$$X = \frac{N_{S1,X}}{N_{st}} \tag{6}$$

with $N_{s1,X}$ the number of moles of hydrated salt in the bed at the advancement X, and $N_{s,t}$ the total number of moles of salt in the bed. X equals 1 when the salt is hydrated and 0 when the salt is dehydrated.

The relationship between the vapor pressure and the temperature of the solid/gas reaction equilibrium and the corresponding liquid/gas water equilibrium are plotted in Figure 1. From the solid/gas reaction equilibrium, Mauran et al [22] determined the standard enthalpy and entropy of the reaction ($\Delta h_r^0 = 67400\ J.mol_G^{-1}$, $\Delta s_r^0 = 175\ J.mol_G^{-1}.K^{-1}$). Moreover, Figure 1 presents an approximate plot of the limit of the saturated solution of $SrBr_2,6H_2O$, calculated by interpolation between two particular points: the melting point of $SrBr_2,6H_2O$ (88.62°C) and its eutectic (-28°C).

According to its bulk density (2390 kg.m^{-3}) and molar mass (0.3555 kg.mol^{-1}) [23], the ideal energy storage density of the hydrated salt S_1 is 629 kWh.m^{-3} (2.27 GJ.m^{-3}). It is 9 times higher than the energy density of liquid water (storage of sensible heat over a 60 K temperature range). Nevertheless, the practical values will be lower because it is necessary to take into account the additional volumes of the gas phase and various parts of the reactor (salt bed porosity, heat exchanger, gas diffuser, dead volumes…).
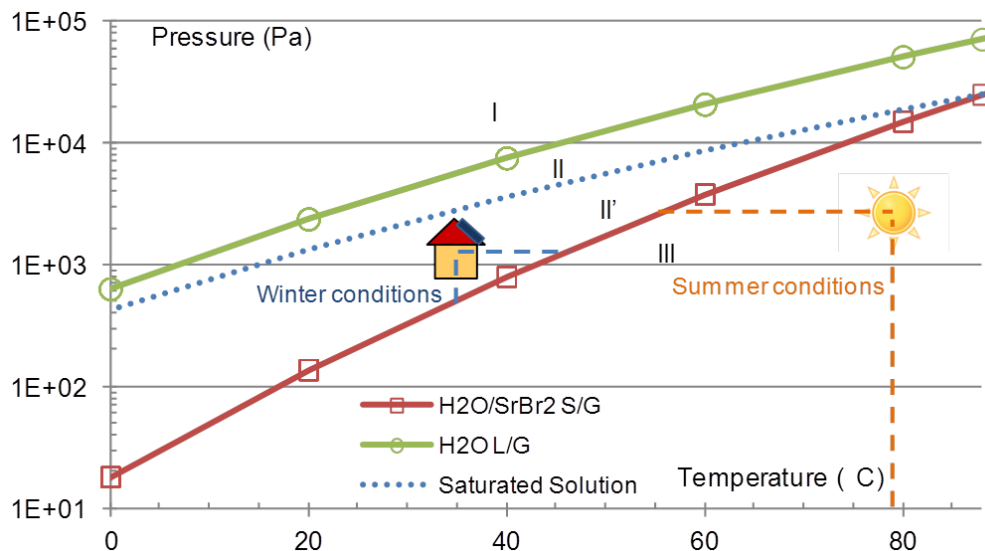
Figure 1: Equilibriums lines of the solid/gas reaction ($SrBr_2$/1-6H_2O) and of the liquid/vapor change (water).
Dotted line: approximate limit of the saturated solution of $SrBr_2,6H_2O$.
Zones I, II, II' and III are respectively the stability zones of: the sub-cooled liquid [H_2O], the sub-cooled saturated solution [H_2O, Sr^{2+}, $2Br^-$] + < $SrBr_2,6H_2O$>, the solid <$SrBr_2,6H_2O$> and the solid <$SrBr_2,1H_2O$>.
The vapor H_2O is super-heated in zones II, II' and III.

2.3. Working mode of the thermochemical seasonal storage process

The thermochemical storage process can operate under pure vapor at low pressure, as explained by Stitou et al [6], or with moist air at atmospheric pressure. As it is technologically difficult to manage the low pressure in a large reactor, we have decided to investigate a system operating with moist air. In that case, the thermodynamic equilibrium conditions (eq. 4) are determined by the partial pressure of water in the moist air.

A thermochemical storage system working with moist air includes a solid/gas reactor containing a porous fixed bed of reactive solid and mass diffusers to distribute the moist air flow through the reactive bed. Thus, the seasonal thermochemical storage for house heating works in the following manner:

- During the heating period (winter): a flow of moist air passes through the dehydrated salt S_0 ($SrBr_2,1H_2O$) within the reactor. The operating conditions (water partial pressure and temperature) are

located in zone II' of Figure 1. Thus, the exothermic synthesis (hydration) of S_0 to S_1 occurs, releasing heat ($5\Delta h_r^0$ per mol of salt) to the moist air flow that acts as heat transfer fluid. This fluid flow then exchanges heat with the house through a gas/gas heat exchanger. At the end of this period, the salt bed is fully hydrated ($SrBr_2,6H_2O$).

- During the storage period (summer): a flow of hot moist air, heated thanks to the heat provided by solar collector, crosses through the porous bed of S_1 ($SrBr_2,6H_2O$). The operating conditions belong to zone III on Figure 1. That leads to an endothermic decomposition reaction (dehydration) of salt S_1 to S_0.

- Between the storage and heating periods, the reactor is closed, and disconnected from the reactive gas flow. That allows to store the reaction heat without energy losses over long time. That makes the thermochemical storage process particularly suitable for seasonal heat storage.

The fact that the reactive gas and the heat transfer fluid are the same fluid adds another advantage for this configuration: it avoids any heat exchangers that would affect the apparent energy density of the storage system.

Another important point for such seasonal storage working is the variation of the partial pressure of water in the ambient air, over the year. Thus, ambient air heated in a solar collector can be used directly to feed the reactor in summer, for the dehydration step. On the other hand, in winter, the water partial pressure of ambient air is too low and it has to be humidified before flowing inside the reactor. Nevertheless, as the following study is focused on materials for thermochemical storage, the temperature and humidity of the inlet moist air are controlled at a constant value.

3. Experimental study of the solid/gas reactive bed

Thermochemical storage processes involve high density salt bed and large amount of moist air passing through it. For both reasons, mass transfer usually strongly limits their working. Thus, an experimentation has been carried out in order to characterize the mass transfer and the reaction kinetics of the porous bed of reactive salt, and the influence of implementation parameters (density, mass ratio binder, diffuser, porous bed texture).

3.1. Experimental set up and protocol

The permeability of the bed (according to Darcy law) and the reaction kinetics are measured in the following experimental bench. The operating principle of the apparatus consists in the measure of the pressure drop across the porous fixed bed and the flowrate of moist air (at controlled humidity and temperature passing through it) through. The kinetics is deduced from the weight variation of the sample.

The experimental bench is composed of a fan, a humidifier, an electric heater and five sample holders (Figure 2). The speed of the fan and the power of the heater are controlled, the humidifier is connected to a thermostatic bath at a controlled temperature. This allows regulating the pressure, temperature and humidity of upstream air of the samples.
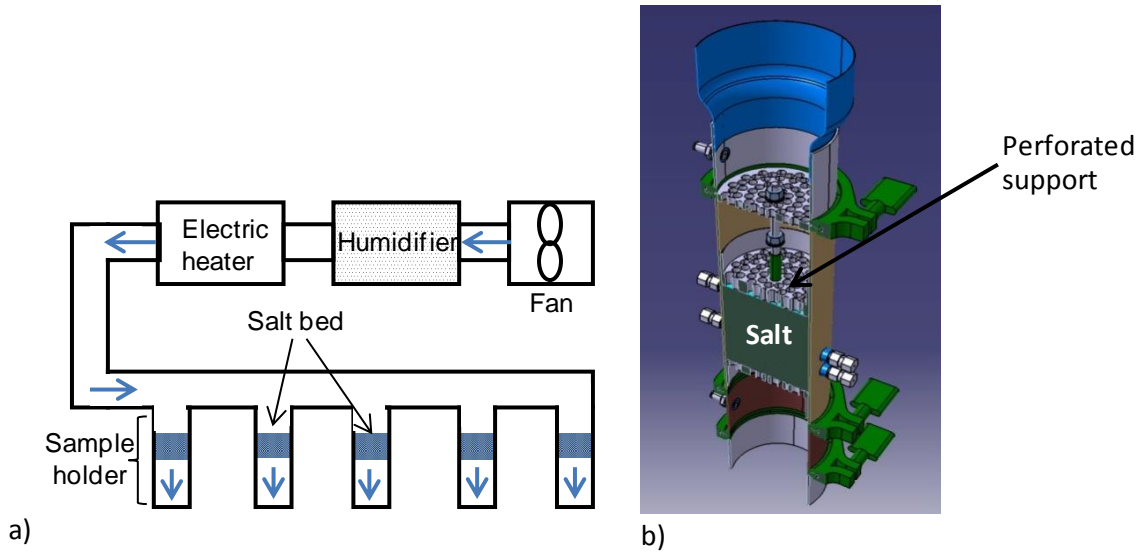
Figure 2: Experimental set-up for mass transfer and kinetics characterizations
a) the experimental bench, b) the sample holder.

The sample holder is a stainless steel tube, 100 mm inner diameter and 467 mm length, insulated by 19 mm of Armaflex (conductivity 0.042 W.m^{-1}.K^{-1}).

The salt is confined between two perforated metallic sheets, the bed thicknesses ranges from 40 to 100 mm. Pressure sensors are located at the bed boundaries, and four thermocouples at different axial coordinates in the salt bed (Figure 2).

It is possible to disassemble the sample holder in order to measure its weight. As the reaction time is long (several days) the disturbances of the reaction kinetics resulting from this weighing is negligible.

During the experimental process, the moist air flows through the sample at given input temperature and humidity. Thanks to the variable speed fan, the inlet pressure of the moist air entering the sample is kept constant, and the outlet pressure is the ambient one. Thus the pressure difference across the salt (∆p) is constant.

Several measurements are recorded during the reaction: the differential pressure at the boundaries of the sample, the flow rate, the temperature and humidity of inlet moist air, the temperatures of the sample, and its mass at given times.

Thus, the equivalent permeability of the whole sample (including the salt bed and the perforated supports) can be deduced from the measurements of the outlet flow rate $\dot{V}$ and the differential pressure across the sample Δp. According to the Darcy's law and assuming an unidirectional flow, in a steady state, and Δp << p, the equivalent permeability is defined as:

$$k_{eq} = \frac{\mu \, Z_{eq} \, \dot{V}}{|\Delta p| \, \Omega} \tag{7}$$

With Ω the cross section of the bed, $Z_{eq} = Z_{sh} + Zs$ the total thickness of the whole set including the perforated supports and the salt bed, and Z_{sh} = 24 mm the thickness of the three successive perforated supports.

Blank experimentations without salt allow to determine the equivalent permeability of the perforated supports: k_{sh} = 1.55.10^{-8} m^2. By an electrical analogy with two flow resistances in series, the permeability of the salt bed (at the reaction advancement X) is expressed as:

6

$$k_X = \frac{Zs}{Z_{eq}/k_{eq} - Z_{sh}/k_{sh}}$$

(8)

The permeability of the dehydrated salt bed (k_0) is measured before starting the hydration reaction. The permeability k_1 of hydrated salt has been measured only for sample 3, because the total reaction requires a rather long time and has only be completed for this sample.

For other cases, k_1 is deduced from the permeability measured during the reaction, assuming that the reaction occurs on a sharp front moving axially through the bed, and separating two layers, one hydrated and the second dehydrated (as detailed in part 4.2). Thus, the permeability k_1 is deduced from the equivalent permeability k_X according to:

$$k_X = \frac{1}{\frac{X}{k_1} + \frac{1-X}{k_0}} \quad \Longleftrightarrow \quad k_1 = \frac{X}{\frac{1}{k_X} - \frac{1-X}{k_0}}$$

(9)

The advancement of the reaction is deduced from the measurement of the weight (m_{sX}) of the sample, according to the following equation:

$$X = \frac{m_{sX} - m_{s0}}{m_{s1} - m_{s0}}$$

(10)

where m_{s0} and m_{s1} are the masses of the dehydrated and hydrated salt bed, respectively. m_{s0} is measured at the hydration beginning and m_{s1} is calculated by the following relation, resulting of the rule of mass additivity:

$$m_{s1} = \frac{m_{s0}}{M_{s0}}(\nu M_\nu + M_{s0})$$

(11)

3.2. Experimental characterizations of the salt bed

Several samples with three kinds of implementations have been tested and characterized in the set up presented in the previous part. The first implementation consists in a bed of salt powder. For the second implementation, a highly porous binder (vermiculite) is added to the salt powder in order to increase the permeability of the sample. The third implementation includes a diffuser (a foam) located at the top of the salt bed.

Only the hydration phases are presented in this paper. The dehydration phases have been carried out with a constraint temperature of 80 °C and Δp = 600 Pa through the bed, but the input humidity was not controlled (ambient humidity).

For the hydration phases, the pressure drop across the sample is fixed (Δp = 500 Pa) and the other operating conditions are listed in Table 1. The inlet partial pressure of water (p_{vi}), the inlet temperature of the moist air (T_{vi}) and the temperature of the sample (T_c), correspond to the average values of these variables measured during the hydrations. The permeabilities calculated for the dehydrated and hydrated salt bed (respectively k_0 and k_1) are presented. The last columns refer to the thickness and the apparent energy density of these samples (excluding perforated supports). The energy density Dec of the reactive bed is defined by the following relation:

$$Dec = n_S \Delta h_r^0$$

(12)

With n_s the molar density of the bed of salt.

Hydration of different samples		p_{vi} (Pa)	T_{vi} (°C)	T_c (°C)	$k_0 *10^{12}$ (m^2)	$k_1 *10^{12}$ (m^2)	Zs (cm)	Dec (kWh.m^{-3})
Sample 1:	1st hydration	1395	23.9	32.7	29.4 ±12.7	8.6 ±3.2		
Sample 1:	2nd hydration	1464	19.9	24.8	98 ±39	7 ±2.4		
Sample 1:	3rd hydration	1322	20.3	28	160 ±79	7.3 ±1.5		
Sample 1:	4th hydration	1181	18.9	23.3	220 ±75	6.7 ±2	4.84	433.5
Sample 1:	5th hydration	1353	17.2	23.1	278 ±115	6.4 ±2		
Sample 1:	6th hydration	982	14.9	19.1	136 ±56	4.8 ±0.9		
Sample 1:	7th hydration	998	17.5	23.9	264 ±144	4.5 ±3.6		
Sample 2: Small grains size		1777	30.5	26.8	24 ±5	0.79 ±0.38	5.81	455.5
Sample 3: Large grains size		1777	30.5	28.8	89 ±34	12.3 ±3.1	5.91	457.7
Sample 4: With vermiculite		1502	12.9	23.5	0.31±0.17	$1.66.10^{-2}$ ±$1.40.10^{-2}$	4.7	507.2
Sample 5: Similar to sample 4 without vermiculite		1397	11.9	22.3	6.8±1.5	0.2 ±0.05	4.7	577.4
Sample 6: With gas diffuser		1214	21.4	22.5	5.6 ±0.9	1.7 ±0.4	5.79	457
Sample 7: Similar to sample 6 without diffuser		1214	21.4	22.8	4.9 ±0.8	0.79 ±0.11	5.99	452.4

Table 1: Operating conditions and characteristics of the reactive salt beds, during hydration phases. The uncertainties on k_0 are calculated from experimental uncertainties on pressure and moist air flowrate, k_1 is calculated from eq. (8) and its uncertainty is deduced from the uncertainties of k_1 and k_X. The masses of samples are in the range 450 to 600 g.

3.3. First implementation: bed of salt powder

3.3.1. The main parameters: permeability and operating conditions

For sample 1, composed of salt powder, seven cycles of hydration / dehydration have been carried out. The operating conditions and the characteristics of the samples are described in Table 1.

The permeabilities as a function of the advancement are plotted in Figure 3 (a) for the seven hydrations of sample 1. The permeabilities are in the range 10^{-10}–10^{-12} m^2 and they don't decrease linearly, but depending on 1/X. This variation of the measured permeability (Figure 3 (a)) can be explained by the assumption of a sharp front of reaction within the salt bed, leading to two distinct layers, one of hydrated salt and the other of dehydrated salt, with different permeabilities. Thus, as described by equation (9), the equivalent permeability of a bed of salt composed of these two layers can be expressed as the following function of 1/X

$$k_X = \frac{k_1 k_0}{X(k_0 - k_1) + k_1}$$ (13)

Results on Table 1 show that the permeabilities of the dehydrated salt bed (k_0) calculated for the first two hydrations are slightly lower than the permeabilities k_0 calculated for the other hydrations. From hydration 3, k_0 is quite stable. On the other hand, the permeability k_1 reduces slightly after each hydration / dehydration cycle, and that could be caused by the fracturing of the salt grains along the successive cycles. Nevertheless, these evolutions are weak compared to the decrease of the permeability during the reaction (Figure 3 (a)).
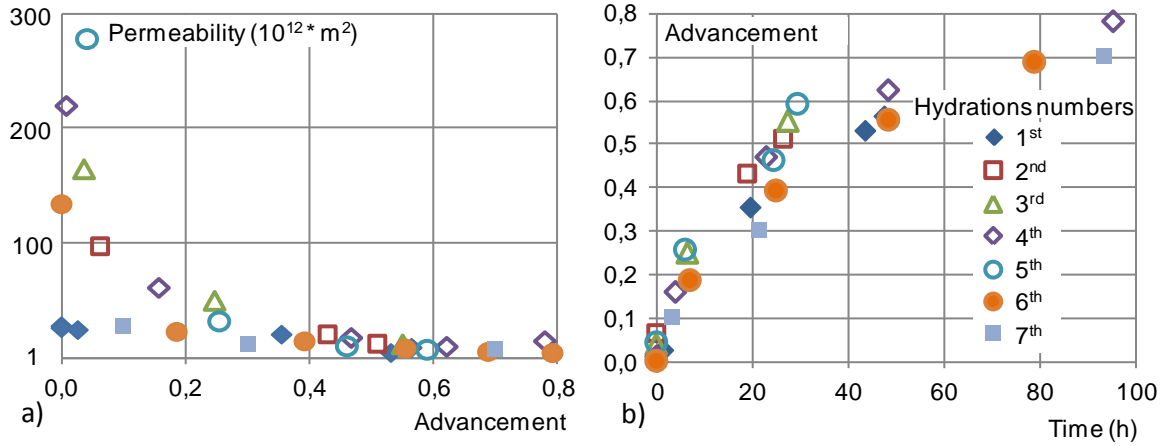
Figure 3: Experimental hydrations of sample 1:
a) permeability k vs. reaction advancement and b) advancement vs. time for seven hydrations

Figure 3 (b) presents the evolution of the reaction advancement vs. time. It displays the usual diminution of the reaction rate vs. advancement for all the hydrations. Nevertheless, the reaction times are rather scattered, and that is mainly visible for advancement beyond 0.4. Hydration 1 differs from others because of its higher temperature Tc. The other hydrations can be roughly distinguished into two groups: the first group includes hydrations 2, 3 and 5, and the second group is composed of hydrations 4, 6 and 7. The reaction rates are slower for group 2 (Figure 3 (b)). For example, the time to achieve a reaction advancement of 0.5 is 40% longer for the second group.

This difference between the two groups is due to the operating conditions, specially the partial pressure of water p_{vi}, (about 1300 Pa and 990 Pa respectively for groups 1 and 2). This lower pressure for group 2 leads to a lower deviation from the thermodynamic equilibrium (at the same temperature Tc). Let's recall that the equilibrium deviation is the deviation between the solid temperature, Tc and the equilibrium temperature of the reaction at the partial pressure of water p_{vi}, and it has an important impact on the reaction time [22].

From the advancement variation vs. time, it's possible to calculate the specific power of the sample at a given advancement X, defined as follows:

$$P_{m_X} = \frac{X \, \Delta h_r^0 \, v}{t_X m_{s0}} \tag{14}$$

with, t_X the reaction time corresponding to the advancement X.

According to Figure 3 (b), the specific power delivered by the sample at a reaction advancement X=0.5 is in the range from 6.8 to 7.2 W/kg for the first group, and from 4 to 5 W/kg for the second group. As the reaction rate decreases with the advancement, the specific power has also to be evaluated at the end of the reaction. At X= 0.78, the hydrations 4 and 6 of sample 1 lead to a specific power of 2.88 W/kg and 1.93 W/kg respectively.

Therefore, in all cases these specific powers are higher than the target values defined in the introduction.

Thus, the sample 1 presents good performances, and specific powers significantly higher than the target values. Moreover, the permeabilities of sample 1 are relatively reproducible over the cycles of reaction. The differences in the reaction times of the various hydrations are mainly due to the different operating conditions and to the resulting equilibrium deviation.

3.3.2. Grains size

Another parameter, that has a great importance on the reaction time, is the texture of the salt bed, especially the size of the grains. Accordingly to the Carman-Kozeny correlation [24] (valid for beds of quite spherical grains), the permeability depends on the diameter of the grains:

$$k_{CK} = \frac{\varepsilon^3 d_g^2}{180(1-\varepsilon)^2}$$

(15)

with d_g the diameter of the grains and ε the porosity of the bed.

Two samples of salt powder (samples 2 and 3), with similar thickness and energy density, but with different sizes of grains have been experimented with the same operating conditions during hydrations (see Table 1). As it can be seen on Figure 4, the sample 2 is made essentially of small grains of salt, which diameter is less than 50 μm, while the sample 3 contains a mixture of larger grains and agglomerations of salt grains.

The apparent porosity of samples 2 and 3 is 64%, at dehydrated state. Assuming a uniform grain size, at 50 μm for sample 2, and 80 μm for sample 3 (see Figure 4 (c) and (d)), the resulting permeability calculated from the Carman-Kozeny correlation for the dehydrated beds are respectively: $k_{0CK, sample2}$ = 28.10^{-12} m^2 and $k_{0CK, sample3}$ = 72.10^{-12} m^2. These values are quite similar to the measured values of the permeabilities of the dehydrated beds (see Table 1).
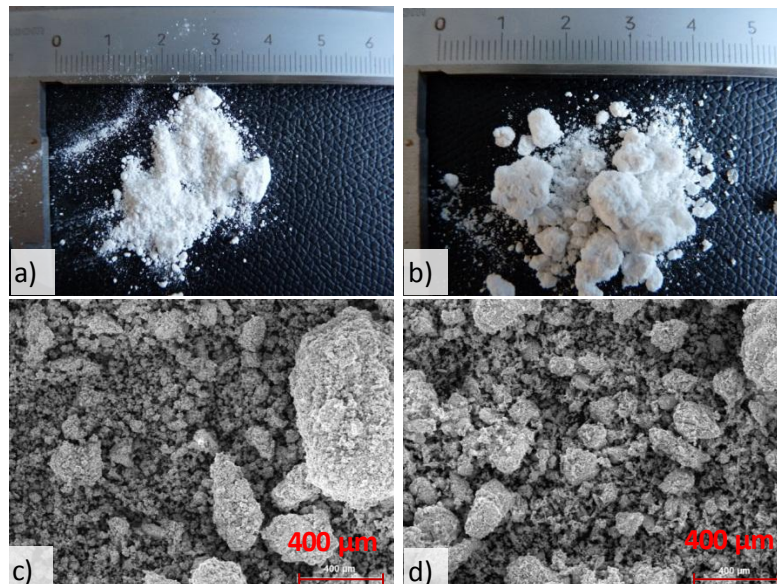

Figure 4: Photographies of a) sample 2 b) sample 3.
Pictures with a scanning electron microscopy (SEM) of c) sample 2, d) sample 3.

Figure 5 presents the reaction advancement as a function of time for samples 2 and 3 during their hydration. One can see that sample 3 reacts faster that sample 2: at 191 hours, sample 3 reaches 86 % of the total reaction, while sample 2 reacted only up to 26 %. These results are consistent with the measured permeabilities in Table 1. The permeabilities of the sample 2 are lower than for sample 3, particularly at the end of reaction, where k_1 is more than 10 times higher for the larger grains (sample 3).

Thus, the texture of the porous bed salt has a great effect on the hydration reaction time. Increasing the size of the salt grains (with all the other parameters constant) allows to increase the permeability, and consequently, to decrease the reaction time.

Moreover, the specific power of sample 3 (with Dec = 457.7 kWh.m^{-3}) is 2.26 W.kg^{-1} for an advancement X=0.78. This is higher than the target values.
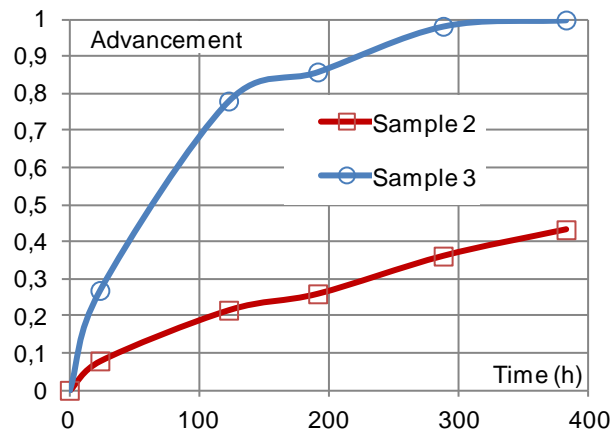
Figure 5: Advancement vs. time for the hydration of sample 2 (small grains) and sample 3 (large grains).

These experimental results show that the hydration of a bed of salt powder leads to satisfactory results: the energy density of the porous bed is about 430-460 kWh.m^{-3} and the specific power at advancement X=0.78 is in the range 1.93 to 2.88 W.kg^{-1}. Moreover, the experimentations of successive cycles of hydration/dehydration for sample 1, demonstrate the reproducibility of performances, and the effect of operating conditions. Finally, the comparison of samples with different grain size has highlighted the importance of the texture of the bed of salt.

To enhance the mass transfer through the salt bed and, as a result, the power released by the reactive bed during hydration, we decided to investigate the addition of a porous non reactive material to be implemented in the salt bed. Two different implementations have been tested and are presented in the following part.

3.4.   Adding a non reactive material

3.4.1.   Hydration of a composite: salt + vermiculite

The addition of a porous binder, supposed to improve mass transfer, has been tested for high density beds. Salt powder has been mixed with a porous binder (exfoliated vermiculite) in sample 4. The binder mass ratio is 5%. It has been compared to a sample of salt powder (sample 5) with the same thickness and a slightly higher energy density (see Table 1).

Figure 6 presents the reaction advancement vs. time for samples 4 and 5. Sample 4 (with vermiculite) has lower energy density than sample 5 (without vermiculite), and its hydration operates with an inlet partial pressure of water slightly higher than for sample 5. Both facts should favor mass transfer in sample 4. Despite that, sample 4 kinetics is strongly slower than sample 5 one: the reaction time to reach a reaction advancement X=0.15 is 238h for sample 4 and 94h for sample 5, i.e. 60% shorter than sample 4.

Moreover, the measured permeabilities of sample 4 are about one order of magnitude lower than sample 5 (see Table 1). Thus, contrarily to the initial objective of this implementation, adding and mixing exfoliated vermiculite with the salt powder decreases the mass transfer and the kinetics of the hydration reaction. Vermiculite is probably compressed during the mixing process with the salt and, leads to add barriers rather than paths for the gas diffusion.
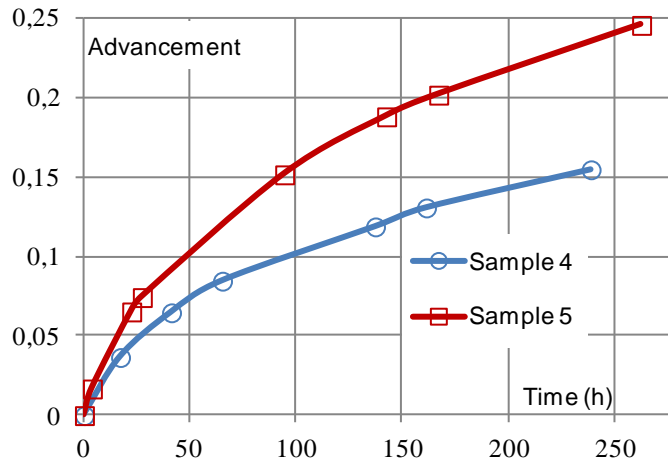
Figure 6: Advancement vs. time for the hydration of sample 4 (507 kWh.m^{-3}, with vermiculite) and sample 5 (577 kWh.m^{-3}, without vermiculite).

3.4.2. Hydration of a bed of salt with a diffuser

Another way to enhance the mass transfer through the bed of powder salt consists in integrating a gas diffuser (foam) at the top of the porous bed (Figure 7). Nevertheless, the diffuser must not pass through the bed of salt, as it would lead to a preferential path for the gas and it would not be able to improve the mass transfer in the whole salt bed.
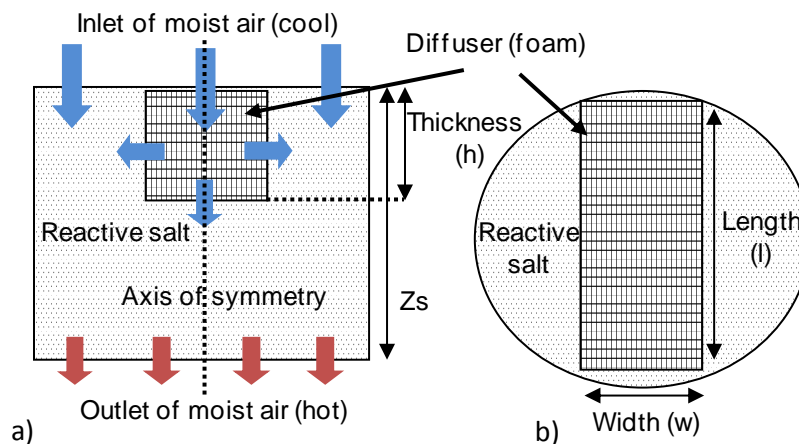
Figure 7: Diagram of a sample of salt bed with a diffuser (size: 98.9 mm x 22.3 mm x 31.4 mm).
a) Vertical sectional view (along the symmetry axis of the sample), b) top view of the sample.

Figure 8 (a) presents the permeability as a function of time for samples 6 (with a gas diffuser) and 7 (without diffuser), during their hydrations. The energy density and operating conditions of the two samples are quite the same (Table 1). Measurements of the apparent permeability lead to higher values for the sample including the gas diffuser (sample 6) than without diffuser (sample 7). The permeability of sample 6 is about 1.7 times greater than permeability of sample 7 (mean value over the reaction). As a result, the sample 6 reacts about 10% faster at X=0.7 than sample 7 (Figure 8 (b)). Thus, this implementation of a gas diffuser allows increasing mass transfer within the salt bed, and leads to a slightly higher specific power of the reactive bed, for the same energy density. The mean value of these specific powers, calculated between X=0 and X=0.55, are 0.3 W/kg and 0.34 W/kg, respectively for sample 7 and 6, thus an increase of 12.5%.
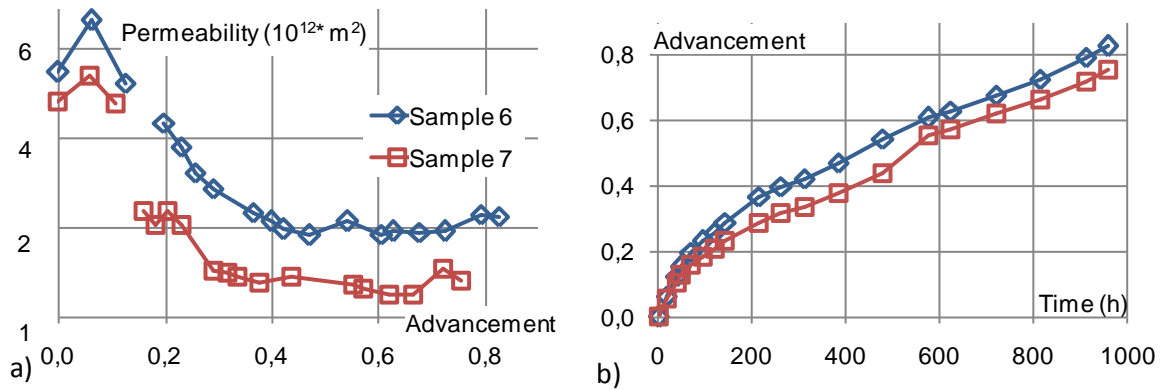
Figure 8: Samples 6 (with gas diffuser) and 7 (without diffuser)
a) Permeability vs. advancement and b) advancement vs. time during hydration.

To conclude, these experimental investigations show that adding an inert porous binder such as vermiculite in the bed of salt doesn't increase the performances of the sample. On the other hand, the implementation of a gas diffuser allows a slight increase of the mass transfer and kinetics during hydration of the reactive bed.

4. Sharp front model

A model of fixed bed transformation has been developed in order to estimate the thermal power involved in a reactive salt bed during hydration and dehydration. The objective is to develop a simple model in order to predict the heat power released during the heating phase and absorbed during the storage phase by the thermochemical storage system working with moist air at atmospheric pressure.
This model takes into account the characteristics of the solid/gas reaction (enthalpy and entropy of reaction), the thermodynamic constraints imposed to the reactor (partial pressure of water, temperature) and the implementation and configuration of the reactive salt in the reactor (thickness, porosity …) which determines the mass transfers characteristics.

4.1. Assumptions

The main assumption of this simple model lies in the existence of a sharp front of reaction. We suppose that the reaction occurs on a sharp front, and this front moves through the reactive bed during the reaction, according to gas diffusion in the bed.
Moreover, as this paper is focused on thermochemical storage process operating with moist air, it requires a high density salt bed and large quantities of no reactive fluid passing through it. Mass transfer can be considered as the main limitation of the reaction, and heat transfer limitation can be neglected. Thus, the model considers only one limitation in the reactor: the mass transfer limitation.
Additional simplifying assumptions are used:
   a)   mass transfer is unidirectional.
   b)   there is no accumulation of heat or gas in the porous volume
   c)   the transformation of the reactant is quasi-static (between the reaction advancement X and X + dX, all physical quantities are constant).
   d)   moist air is considered as an ideal gas.
   e)   the kinetics is not limiting, thus the thermodynamic equilibrium is assumed at the reaction front.
   f)   Assuming that heat transfer is not limiting, the temperature of the bed of salt is uniform and equals to the constraint temperature T_c.

A variant of the proposed model (with two reaction fronts) has already been applied and validated for thermochemical process operating under pure vapor, in the case of a solid/gas reaction involving reactive pair $MnCl_2/NH_3$ (Lu et al [25]), and $SrBr_2/H_2O$ (Lahmidi et al [8]).

4.2. Geometric configuration

We consider a porous bed of reactive salt (Figure 9). Its total thickness Zs. Does not vary during reaction because the bed is confined between two perforated metallic sheets.
Let's first describe the model for hydration phase.
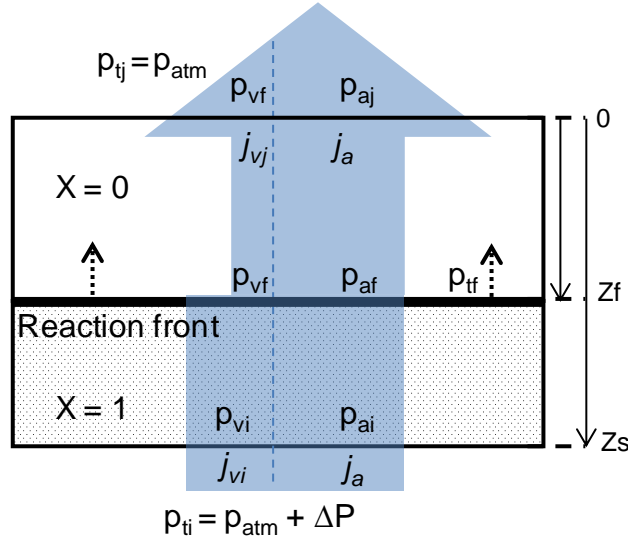
Figure 9: Schematic representation of the porous bed of reactive salt, crossed by a flow of moist air.

The total inlet molar flow is $j_{hi} = j_a + j_{vi}$. The bed is submitted to a pressure difference Δp between its boundaries. The flow of moist air through the reactive layer and the partial pressures of dry air and water in this flow are described schematically in Figure 9.
The salt reacts with water vapor at the sharp reaction front, at Zf. Zf varies from Zs to 0 during the hydration reaction. Thus, this front separates two layers in the bed: between 0 and Zf the salt is dehydrated (X = 0) and between Zf and Zs, the salt is hydrated (X = 1). The reaction advancement X is defined by following equation:

$$X = 1 - \frac{Zf}{Zs}$$ (16)

On the reaction front, the thermodynamic equilibrium is assumed. Therefore, the partial pressure of water is calculated from the Clausius-Clapeyron relation (eq. 4) and the bed temperature T_c:

$$p_{vf} = p_{eqSG} = p^0 e^{-\frac{\Delta h_r^0}{RT_c} + \frac{\Delta s_r^0}{R}}$$ (17)

Moreover, we can evaluate the following pressures:
- the partial pressure of water at the inlet of the reactive bed is fixed : $p_{vi} = p_{eqLG}(T)$.
- the partial pressure of water between the front and the outlet of the bed is kept constant : $p_{vj} = p_{vf.}$
- the total pressure at the outlet of the reactive bed is measured: $p_{tj} = p_{atm}$

4.3. Model equations

For sake of simplicity, the equations are detailed only for the hydration. The dehydration equations follow the same principle.

4.3.1. Molar balance

The molar balance of the moist air in the porous bed of reactive salt is writing as:

$$\frac{\partial(\varepsilon n_h)}{\partial t} = \dot{n} - \nabla \cdot [j_h],$$ (18)

With j_h the molar flux of moist air (mol.m^{-2}.s^{-1}), given by the Darcy law and $\dot{n}$ the gas sink or source due to the reaction:

$$\begin{cases} j_h = -n_h \frac{k_s}{\mu} \nabla p \\ \dot{n} = -v n_S \frac{dX}{dt} \end{cases}$$ (19)

Nevertheless, considering that there is no accumulation of heat or gas in the porous volume (assumption b), the mass balance can be expressed as:

$$\nabla \cdot [j_h] = -v n_S \frac{dX}{dt}$$ (20)

Moreover, as the mass transfer is unidirectional (assumption a), eq. (20) becomes:

$$\frac{d}{dz} \cdot [j_{hz}] = -v n_S \frac{dX}{dt},$$ (21)

With j_{hz} the molar flux in the z direction, given by the following equation:

$$j_{hz} = -n_h \frac{k_s}{\mu} \frac{dp}{dz}$$ (22)

The integration of the equation (21) between the inlet and the outlet of the salt bed gives the following equation of the kinetics of the reaction:

$$\int_i^j \frac{-dj_{hz}}{v n_S} = \frac{j_{hi} - j_{hj}}{v n_S} = \int_i^j \frac{dX}{dt} dz = \frac{dX}{dt} Zs$$ (23)

The moist air is composed of dry air and vapor. The molar flow of moist air is: $j_h = j_a + j_v$. Moreover, we consider that the dry air flow is constant between the inlet and the outlet of the salt bed $(j_{ai} = j_{aj} = j_a)$. The reaction rate (eq. (23)) becomes:

$$\frac{dX}{dt} = \frac{j_{vi} - j_{vj}}{Zs\, v\, n_S}$$ (24)

4.3.2. Moist air flow and partial pressures across the porous salt bed

To calculate the reaction time, it is necessary to determine the flow of vapor at the inlet j_{vi} and the outlet j_{vj} of the reactive bed. Thanks to the assumption of a sharp front of reaction, it is possible to calculate the vapor flow in the two layers (see Figure 9). As the pressure gradient across the bed is small compared to the total pressure, we can consider the moist air as an incompressible fluid.
Thus, for the hydrated layer (from Zs to Zf), the Darcy equation on the moist air can be written as:

$$u = \frac{\dot{V}}{\Omega} = \frac{k_1}{\mu} \frac{p_{ti} - p_{tf}}{Zs - Zf}$$ (25)

Considering that the moist air is an ideal gas, the flow becomes:

$$\frac{\dot{V}}{\Omega} = \frac{j_a + j_{vi}}{p_{ti}} RT_c$$ (26)

Combining equations (16), (25), and (26), leads to:

$$j_a + j_{vi} = \frac{k_1 \, p_{ti}}{R \, T_c \, \mu \, X \, Zs} (p_{ti} - p_{tf})$$

(27)

Similarly, for the dehydrated layer (from 0 to Zf):

$$j_a + j_{vj} = \frac{k_0 \, p_{ti}}{R \, T_c \, \mu \, (1-X)Zs} (p_{tf} - p_{tj})$$

(28)

Equations (27) and (28) defining j_{vi} and j_{vj} involve news unknown (p_{tf} and j_a) and require additional equations:

- the relationship between partial pressures and molar flow rates, at the input and output of the bed:

Input: $\dfrac{j_a}{j_a + j_{vi}} = \dfrac{p_{ai}}{p_{ti}}$

(29)

Output: $\dfrac{j_a}{j_a + j_{vj}} = \dfrac{p_{aj}}{p_{tj}} = \dfrac{p_{aj}}{p_{atm}}$

(30)

The total pressure at the reaction front is:

$$p_{tf} = p_{vf} + p_{af}$$

(31)

From the equations (27) to (31) and pressure values defined in part 4.2, it is possible to determine the flow of vapor at the inlet j_{vi} and the outlet j_{vj} of the bed of salt, and the whole set of pressure in the bed.

4.3.3. Reaction time

The equation (24) of the reaction rate is integrated between X = 0 and X_t, using the resolution of the system of five equations (equations (27) to (31)) with 5 unknowns (p_{tf}, p_{af}, j_a, j_{vi}, j_{vj}). It allows to obtain the time required to reach a given reaction advancement X for the porous reactive salt bed.

$$\Delta t_{X_t} = A X_t \left(p_{ai} k_1 - \left(p_{ai} k_1 - p_{aj} k_0 \right) \frac{X_t}{2} \right)$$

(32)

With:

$$A = \frac{Zs^2 R \, T_c \, \mu \, n_S}{k_1 \, k_0 \left[(p_{ti} - p_{tj})(p_{aj} \, p_{ti} - p_{ai} \, p_{tj}) \right]} = \frac{Zs^2 R \, T_c \, \mu \, Dec}{\Delta h_r^0 \, k_1 \, k_0 \left[(p_{ti} - p_{tj})(p_{aj} \, p_{ti} - p_{ai} \, p_{tj}) \right]}$$

(33)

The second expression involves the main characteristic of the storage material: the energy density Dec of the reactive bed (eq. 12)
In dehydration the advancement of reaction varies from 1 to 0. And with the same method we obtain the following reaction time:

$$\Delta t_{X_t} = A(X_t - 1) \left(p_{aj} k_1 + \left(p_{ai} k_0 - p_{aj} k_1 \right) \frac{X_t + 1}{2} \right)$$

(34)

5. Comparison between model and experimental results

This part compares simulations resulting from the sharp front model and experimental results. The simulations are carried out using the characteristics measured for each sample (Dec, Zs, k_1 and k_0), and the experimental operating conditions for each hydration (p_{vi} and T_c, see Table 1). Typical results are presented in the following figures.

For sample 1, the comparison of the reaction advancement vs. time for hydrations 2, 3 and 7 are presented on Figure 10. The mean value of the relative deviation between experimentations and the model results are 6%, 5% and 10% respectively for hydrations 2, 3 and 7. Let's recall that this set of hydrations represents the whole range of operating conditions listed in Table 1.

Thus, the sharp front model predicts correctly the reaction advancement evolution for the hydration of a porous bed of salt.
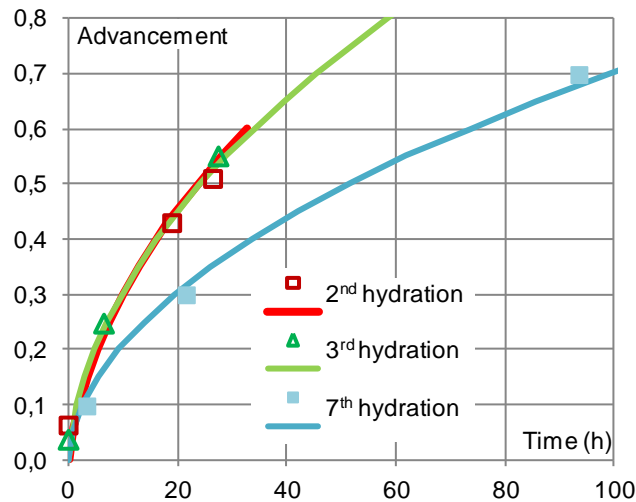
Figure 10: Advancement vs. time for hydrations 2, 3 and 7 of sample 1: experimental results (symbols) and simulations using the sharp front model (line).

On the other hand, experimental and simulated results for sample 6 (with gas diffuser) and 7 (without diffuser) are compared on Figure 11. We observe that the sharp front model predicts fairly well the hydration time for sample 7 (without diffuser), between X = 0.16 and X = 0.75. The mean relative deviation in this large range of advancement is 13%. On the other hand, it doesn't predict correctly the hydration reaction time of sample 6. Indeed, according to the geometry of sample 6 (Figure 7), the mass transfers in the top part of this reactive bed cannot be considered as unidirectional (assumption a).
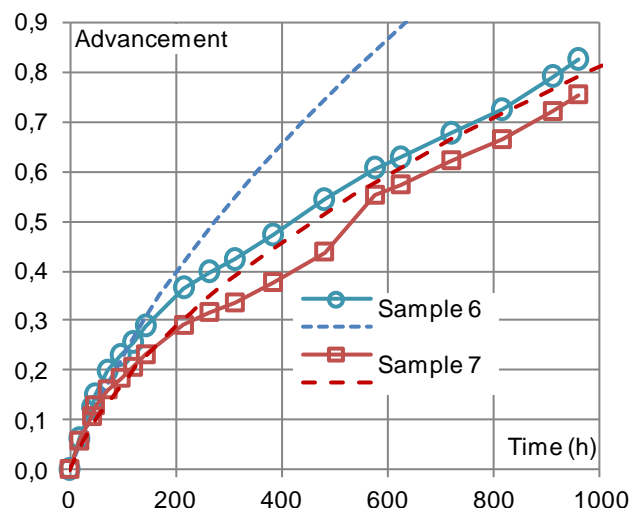
Figure 11: Advancement vs. time for hydrations for samples 6 (with gas diffuser) and 7 (without diffuser): experimental results (symbols) and simulations using the sharp front model (dotted line).

Thus, the sharp front model is a simple and efficient tool to predict quite correctly the reaction time for the porous bed of salt powder with high density, with respect to assumptions described in part 4.1.

6. Conclusion

This work aims at estimating in order to later optimize the performances of a seasonal thermochemical storage process, based on solid/gas reaction in a fixed bed configuration. First, it focuses on the characterizations of mass transfer within the reactive salt bed, and on the different implementation parameters (density, binder, diffuser, porous bed texture) that could enhance the performances (energy density, specific power). Secondly, a simulation tool has been developed to represent the reaction in the reactive salt bed, and to estimate the thermal power.

Hydrations of salt beds have been experimented for various operating thermodynamic conditions and densities. They lead to good results: an energy density of about 430-460 kWh.m^{-3}; a specific power between 1.93 and 2.88 W.kg^{-1} at the advancement X=0.78, and more than two times higher at mid-reaction (X=0.5). It is higher than the target value (0.35-0.7 W.kg^{-1}) defined in a previous study for typical French climate and houses [17]. Moreover, the reproducibility of the results was demonstrated. The effects of the operating conditions and the size of the salt grains were also highlighted.

To enhance the mass transfer through the salt bed, various implementations have been investigated. A porous binder and a gas diffuser have been added. The experiments show that the selected binder (highly porous vermiculite) doesn't allow any reduction of the reaction time, and, as a result, it doesn't lead to any enhancement of the thermal power. On the other hand, adding a gas diffuser in the top part of the salt bed leads to a slight increase of the performances of bed during hydration.

A model has been developed in order to represent the solid/gas thermochemical reaction in a porous bed with a flow of moist air and, consequently, to estimate the thermal power. The model is based on the assumption of a sharp reaction front moving through the bed during the reaction, and, separating the reacted and un-reacted parts of the bed. The comparison between the model and experimental results validates the sharp reaction front model. It demonstrates that this tool is simple and very efficient to predict the transformation of high density porous reactive beds, as long as the assumption of unidirectional mass transfers is respected. A more complex 2D model is currently developed for more complex geometries.

The next step in progress is the design and the test of a prototype of thermochemical storage at a significant scale (about 400 kg of salt powder, represents 105 kWh). The reactor conception has to be simple and compact. The test of this prototype will allow to demonstrate the feasibility of seasonal thermochemical storage process with a fixed bed configuration and functioning with moist air for house heating application.

Acknowledgements

References:

[1] ademe.fr [Internet]. Agence de l'Environnement et de la Maîtrise de l'Energie; c2012 [cited 2012 April]. L'efficacité énergétique des bâtiments, contexte et enjeux; Available from: http://www2.ademe.fr.

[2] Pinel P, Cruickshank CA, Beausoleil-Morrison I, Wills A. A review of available methods for seasonal storage of solar thermal energy in residential applications. Renewable and Sustainable Energy Reviews. 2011;15:3341-3359.

[3] N'Tsoukpoe KE, Liu H, Le Pierrès N, Luo L. A review on long-term sorption solar energy storage. Renewable and Sustainable Energy Reviews. 2009;13:2385-2396.

[4] Hadorn J-C. Advanced storage concepts for active solar energy—IEA SHC Task 32 2003-2007. In: Eurosun—1st international conference on solar heating, cooling and buildings. Lisbon. October 2008.

[5] Mauran S, Lahmidi H, Goetz V. Solar heating and cooling by a thermochemical process. First experiments of a prototype storing 60 kWh by a solid-gas reaction. Solar Energy. 2008;82:623-636.

[6] Stitou D, Mazet N, Mauran S. Experimental investigation of a solid/gas thermochemical storage process for solar air-conditioning. Energy. 2012;41:261-270.

[7] Jaehnig D, Hausner R, Wagner W., Isaksson C. Thermo-chemical storage for solar space heating in single-family house. In Proceeding of Ecostock. New Jersey, May 2006.

[8] Lahmidi H, Mauran S, Goetz V. Definition, test and simulation of a thermochemical storage process adapted to solar thermal systems. Solar Energy. 2006;80:883-893.

[9] Boer R, Haije W, Veldhuis J, Smeding S. Solid sorption cooling with integrated storage: the SWEAT prototype, In 3rd international heat powered cycles conference—HPC. 2004.

[10] Iammak K, Wongsuwan W, Kiatsiriroj T. Investigation of modular chemical energy storage performance. In The joint international conference on sustainable energy and environment (SEE). 2004.

[11] Kerskes H. Seasonal sorption heat storage. in DANVAK seminar (solar heating systems – Combisystems – heat storage). DTU Lyngby, 14 November 2006.

[12] Hauer A, Lävemann E. Open absorption systems for air conditionning and themal energy storage, Thermal energy storage for sustainable energy consumption. Netherlands: Springer. 2007:429-44.

[13] Bertsch F, Mette B. Asenbeck S, Kerskes H, Müller-Steinhagen H. Low temperature chemical heat storage – an investigation of hydration reactions. In Proceeding of Effstock. Stockholm, 2009.

[14] Zondag H, Kikkert B, Smeding S, De Boer R, Bakker M. Prototype thermochemical heat storage with open reactor system. In Proceeding of the 12th International Conference on Energy Storage-Innostock 2012. Lleida, Spain, 2012.

[15] Marias F, Tanguy G, Wynttenbach J, Rouge S, Papillon P; Thermochemical storage: first results of pilot storage with moist air. In Proceeding of ISES. Kassel, Germany, 2011.

[16] Haji Abedin A, Rosen MA. Closed and open thermochemical energy storage : Energy- and exergy-based comparisons. Energy. 2012;41(1):83-92.

[17] Tanguy G, Papillon P, Paulus C. Seasonal storage coupled to solar combisystem: dynamic simulations for process dimensioning. In Proceeding of Eurosun. Graz, Austria, 2010.

[18] Tanguy G, Papillon P, Paulus C. Solar combisystem and storage: the way to achieve high solar fraction. In Proceeding of IRES. Berlin, 2009.

[19] Stitou D, Mazet N, Bonnissel M. Performance of a high temperature hydrate solid/gas sorption heat pump used as topping cycle for cascaded sorption chillers. Energy. 2004;29(2):267-285.

[20] Le Pierrès N, Mazet N, Stitou D. Experimental results of a solar powered cooling system at low temperature. International Journal of Refrigeration. 2007;30(6):1050-8.

[21] Lu H, Mazet N. Mass-transfer parameters in gas-solid reactive media to identify permeability of IMPEX. AICHE. 1999;45(11):2444-2453.

[22] Mauran S, Lahmidi H, Goetz V, 3rd Intermediate Report, European project no NNE5-2000-00385. 2002.

[23] D. R. L., Handbook of Chemistry and Physics 78th Edition. 1997-1998.

[24] Carman P. Flow of gases through porous media. Londres: Butterworths, 1956.

[25] Lu H, Mazet N, Coudeville O, Mauran S. Comparison of a general model with a simplified approach for the transformation of solid–gas media used in chemical heat transformers. Chemical Engineering Science. 1997;52(2):311–327.